

# Microstructure and Pitting Corrosion Resistance of Titanizing Coating Prepared by Pack Cementation on 316L Stainless Steel

Minhang Zeng, Yong Yang\*, Moucheng Li\*

Institute of materials, School of Materials Science and Engineering, Shanghai University, 149 Yanchang Road, Shanghai 200072, China

\*E-mail: [yangongy@163.com](mailto:yangongy@163.com) (Y. Yang), [mouchengli@shu.edu.cn](mailto:mouchengli@shu.edu.cn) (M.C. Li)

Received: 16 March 2021 / Accepted: 24 April 2021 / Published: 31 May 2021

---

Titanizing coatings were prepared on 316L stainless steel by the pack cementation method at 950, 1020 and 1100 °C. The coating surface and cross-section were analyzed by using X-ray diffraction (XRD) and scanning electron microscopy (SEM). The electrochemical corrosion behavior in 3.5% NaCl solution at 80 °C was measured through electrochemical techniques. The results showed that titanium coatings were continuously generated on the 316L substrate at different treatment temperatures. The coatings were composed of NiTi<sub>2</sub>, FeTi, NiTi, Ti and δ-ferrite phases through the diffusion process. The titanium coatings displayed much higher polarization resistance and pitting resistance than 316L stainless steel in the hot seawater. The pitting potential reached approximately 950 mV<sub>SCE</sub> with an increase in the titanization temperature from 950 to 1100 °C.

---

**Keywords:** 316L stainless steel; titanizing coating; pack cementation; pitting corrosion

## 1. INTRODUCTION

Type 316L stainless steel (SS) is widely applied in the food, furniture, medical appliances and chemical industries due to its good corrosion resistance [1, 2]. The excellent corrosion resistance of stainless steel is primarily due to the protective passive film formed on the surface. However, the protective layer is susceptible to localized breakdown when stainless steel is exposed to an aggressive environment containing Cl<sup>-</sup> ions. As one of the most common kinds of localized corrosion, pitting corrosion will lead to the deterioration of the strength of materials and the stress concentration around the pits, thereby accelerating the failure of SS materials [3]. Therefore, the application of 316L SS is limited to some extent.

Pack cementation is an effective and convenient approach to fabricate protective diffusion coatings [4]. In general, the specimen is buried in a powder mixture composed of insert fillers, master alloy elements and activators. The metal halide generated at high temperature diffuses into the specimen

surface and forms a protective layer through interdiffusion effect with the substrate [5]. This kind of in-situ chemical vapor deposition process has been extensively used in the fabrication of aluminizing, chromizing and siliconizing coatings due to the low cost and the tight adhesion between the coating and the substrate at high temperature [5, 6]. It has been reported that the addition of Ti can improve the corrosion resistance of metallic materials by enhancing the protectiveness of passive films [7]. Lin et al. prepared a titanizing coating on 316SS via pack cementation, resulting in a significant increase of pitting potential in a 3.5% NaCl solution [8]. Xing et al. successfully fabricated a rare earth modified titanizing coating on 304SS in a nonprotective atmosphere through two-step pack cementation, which remarkably improved the corrosion resistance of the substrate [9].

Considering the aggressive environment of hot seawater [10], this work aims to investigate the influence of temperature on the microstructure and pitting resistance of the titanizing coating via SEM, XRD and electrochemical techniques. This study will provide fundamental information for improving the corrosion resistance of stainless steels in hot seawater environments.

## 2. EXPERIMENTAL

### 2.1 Preparation of titanizing coating

Commercial 316L SS with the chemical composition in Table 1 was used as the substrate. The 6 mm thick specimens were cut into 11×11 mm pieces by electrical discharge machining, cleaned with acetone and abraded with SiC papers to 1500-grit. After that, the specimens were ultrasonically cleaned in anhydrous ethanol and dried for later use.

**Table 1.** Chemical composition of 316L SS (wt. %)

Cr	Ni	Mo	Si	C	P	Fe
16.4	10.3	2.05	0.57	0.023	0.034	Bal.

A high temperature low-activity process was adopted in this study. The pack mixtures comprised titanium sponge (99.7% purity, grit 50  $\mu\text{m}$ ),  $\alpha\text{-Al}_2\text{O}_3$  powder (99% purity, grit 5  $\mu\text{m}$ ) and  $\text{NH}_4\text{Cl}$  (as an activator) with mass fractions of 57%, 40% and 3%, respectively. Before the preparation of the mixtures, the  $\text{NH}_4\text{Cl}$  particles were dehydrated in a ventilation oven and finely ground. The mixture powders were homogeneously mixed by grinding in an alumina mortar for 20 min. The 316L SS specimen was placed in the middle of a cylindrical alumina crucible and packed by filling the powder mixtures around it. Only one specimen was treated in each alumina crucible. Next, every alumina crucible was covered with an aluminide lid and sealed with high-temperature cements to prevent the mixtures from being oxidized under high temperature conditions. The cement sealants were first cured for 24 h at ambient temperature and then transferred into a vertical furnace and heated to 150  $^\circ\text{C}$  for 3 h to further remove moisture from the cements. The temperature was then rapidly raised to the target temperature (950, 1020 and 1100  $^\circ\text{C}$ ),

and the pack cementation process was conducted for 3 h. After the reaction, the furnace was cooled to ambient temperature at a natural rate. The back of the specimen used for the electrochemical test was ground with SiC paper and welded to a copper wire. The specimens were then embedded in epoxy resin with a working area of 1 cm<sup>2</sup>.

## 2.2 Electrochemical measurements

All electrochemical measurements were performed in a conventional three-electrode cell with a Model 273A Potentiostat/Galvanostat with a lock-in amplifier (M5210) and Powersuit software. The specimen was used as the working electrode, and a saturated calomel electrode (SCE) and a platinum plate were used as the reference electrode and the counter electrode, respectively. All the tests were conducted in a 3.5 wt% NaCl solution at 80 °C with a pH value of approximately 7 [9,10]. After the specimen was immersed in the test solution, the open circuit potential (OCP) was first measured for 1 h to reach a relatively steady state. Next, electrochemical impedance spectroscopy (EIS) measurements were performed with an AC disturbance signal of 10 mV (rms) in the frequency range from 99000 to 0.01 Hz. The impedance data were fitted utilizing ZSimpWin software. Finally, the cyclic anodic polarization experiment was performed from the OCP with a scan rate of 20 mV·min<sup>-1</sup>. The potential scan was reversed when the current density reached 1 mA·cm<sup>-2</sup>. The electrochemical tests were repeated three times to ensure the reliability of the results.

## 2.3 Coating analysis

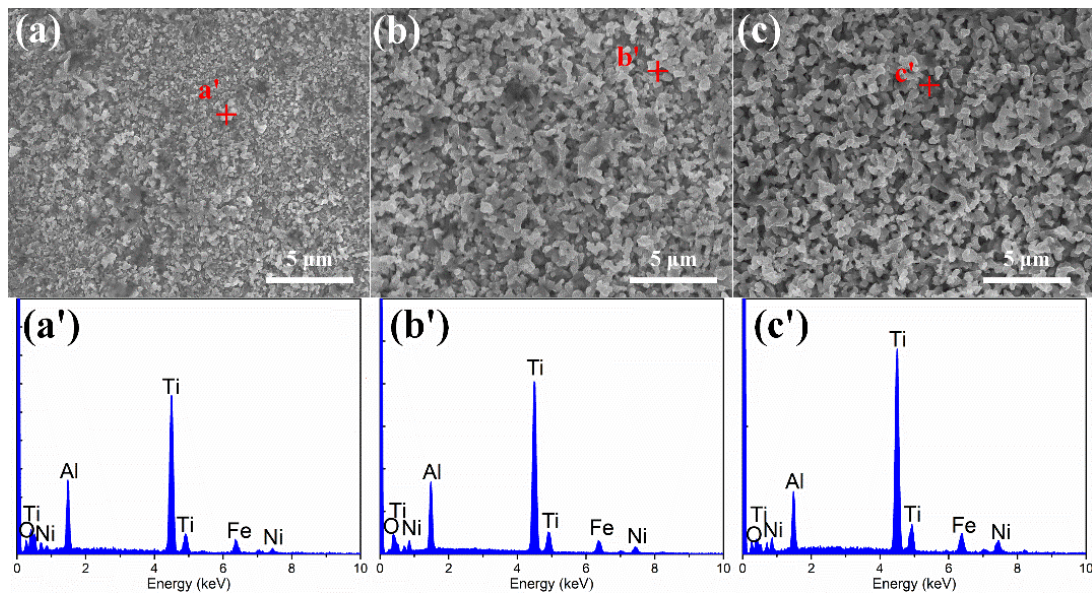
The phase composition of the titanizing coating was analyzed with X-ray diffraction by using a Rigaku diffractometer (D/MAX 2550 V) with Cu Ka radiation at 40 kV. Field emission scanning electron microscopy (SEM, Joel JSM-7500F) with energy-dispersive X-ray spectroscopy (EDS) was used to characterize the surface and cross-section microstructures of the coating and the corresponding chemical composition, as well as the specimen surfaces after the cyclic anodic polarization measurements.

# 3. RESULTS AND DISCUSSION

## 3.1 Microstructure characteristics

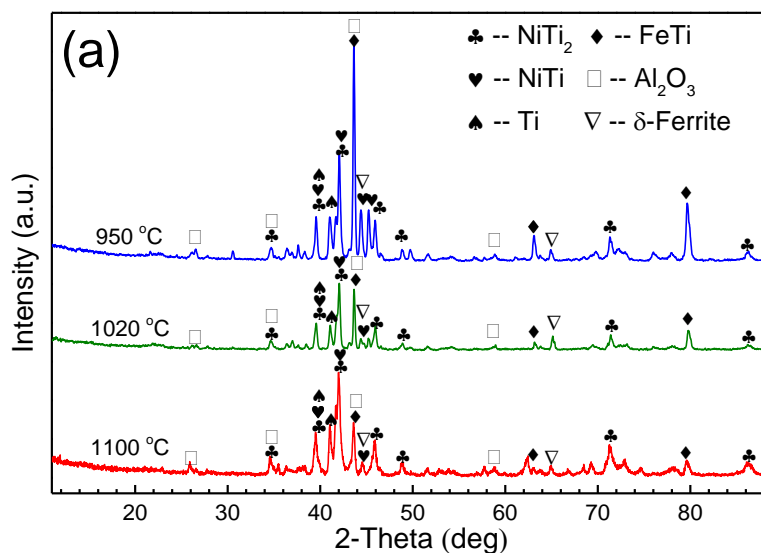
Fig. 1 presents the SEM morphologies and EDS analyses of the 316L SS surfaces after pack cementation at different temperatures. All the titanizing coatings present an “ant hole-like” structure with many micropores on the surface, which can be attributed to the combined effect of vacancy migration and the diffusion of Ti into the substrate, as well as the penetration of the gas generated by NH<sub>4</sub>Cl decomposition into the coatings at high temperature [8, 11]. In addition, the “ant hole-like” structure is very loose with poor bonding force with the inner layer of coatings, which is easy to remove

by polishing. The EDS results show that the chemical composition of the coating surfaces mainly consist of Ti, Fe, Ni, Al and O elements.



**Figure 1.** SEM-EDS analysis of the 316L SS surface after pack cementation at different temperatures: (a, a') 950 °C, (b, b') 1020 °C and (c, c') 1100 °C.

Fig. 2(a) shows the XRD patterns of titanizing coatings prepared at different temperatures. The response peaks indicate that the main components of the coatings are identified as intermetallic compounds  $\text{NiTi}_2$ ,  $\text{FeTi}$ , and  $\text{NiTi}$ , with the appearance of  $\text{Al}_2\text{O}_3$ ,  $\delta$ -ferrite and metallic Ti phases.



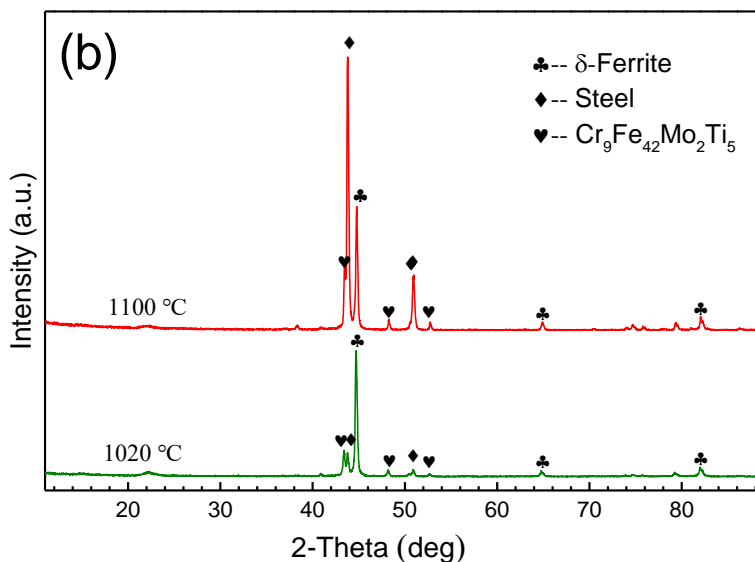


**Figure 2.** XRD patterns of titanizing coatings: (a) outer layer and (b) inner layer

There is no response from the 316L SS substrate, which may be attributed to the limited diffraction depth of X-rays in the outer layers. Fig. 2(b) shows the XRD patterns for the inner layer of the coatings formed at 1020 and 1100 °C, which were obtained after removing the outermost layers of coatings by slow grinding.  $\delta$ -ferrite and  $\text{Cr}_{13}\text{Fe}_{42}\text{Mo}_2\text{Ti}_5$  phases appear in the inner layers close to the 316L SS substrates.

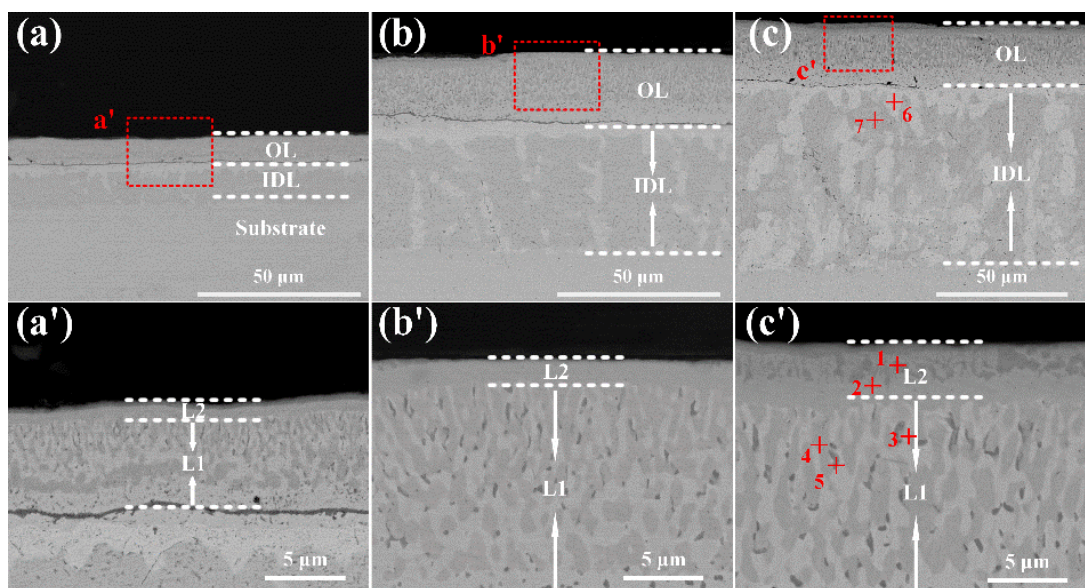


**Figure 3.** SEM cross-sectional morphologies of titanizing coatings: (a, a') 950 °C, (b, b') 1020 °C and (c, c') 1100 °C.

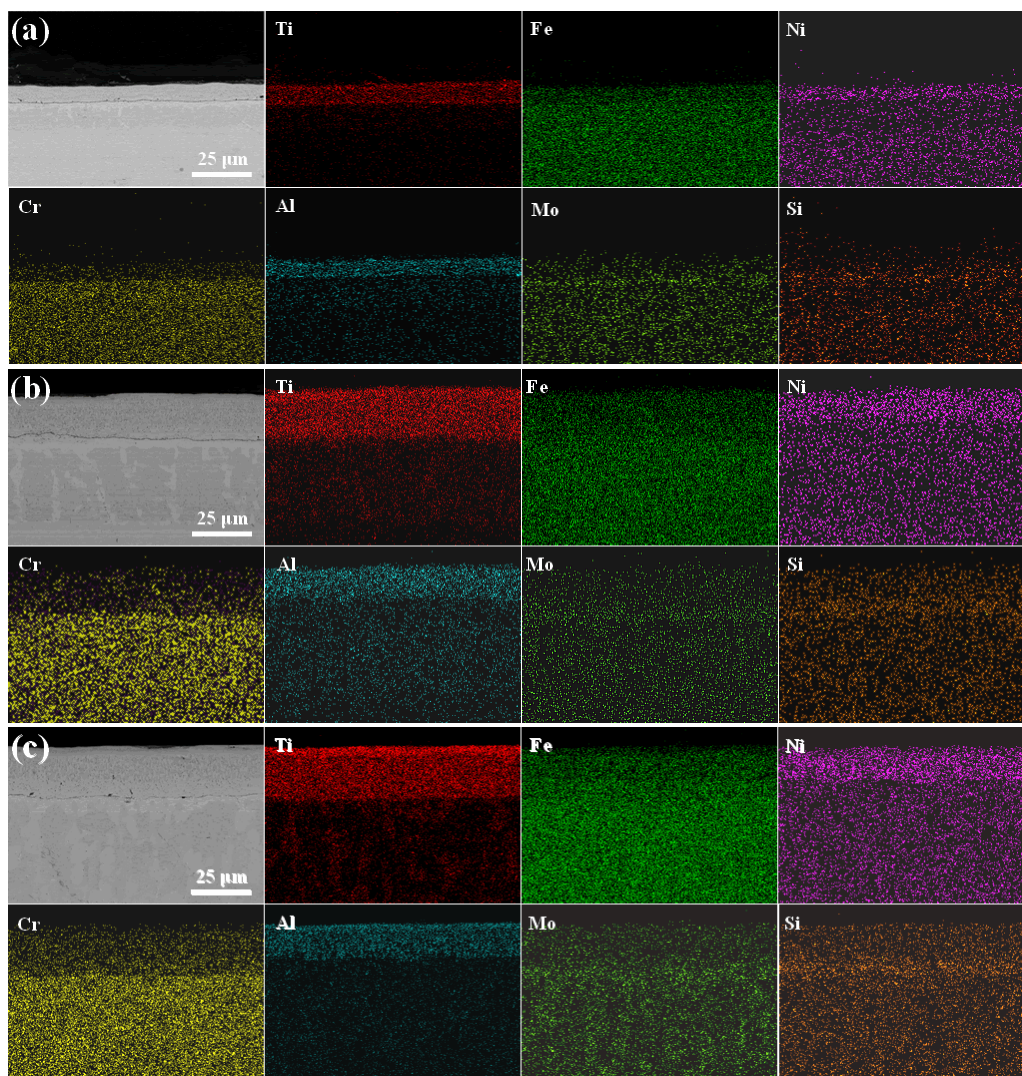


**Figure 4.** Element distribution in the cross sections of titanizing coatings: (a, a') 950 °C, (b, b') 1020 °C and (c, c') 1100 °C.

Fig. 3 presents the SEM cross-sectional morphologies of the titanizing coatings after the removal of the loose layer by polishing slightly. It is apparent that the titanizing coatings show a complex but continuous and very dense structure without obvious micropores, and more than one phase region is observed in the coatings. The thickness of the coating increases from approximately 20 to 94  $\mu\text{m}$  when changing the temperature from 950 to 1100 °C. Moreover, the titanizing coatings formed at different temperatures exhibit similar microstructures and good adhesion with the substrate.

Fig. 4 shows the elemental distribution in the cross sections of the coatings after slight polishing. The interdiffusion of metal atoms can be seen under high temperature conditions, that is, Ni and Fe atoms diffuse outwards from the substrate whereas Ti atoms diffuse in the opposite direction. At the same time, the diffusion of Cr, Mo and Si atoms also takes place. Ni is enriched in the outer layer through an uphill diffusion process, whereas Mo and Si are concentrated at the original surface of the 316L substrate due to the high temperature effect. In addition, Al is also found in the coatings.

It is apparent that the temperature can influence the titanizing coating thickness, but has little effect on the phase composition and microstructure. The titanizing coating formed at 1100 °C is adopted as an example to further analyze the chemical composition of the individual phase region, as listed in Table 2. The EDS mapping results indicate that the titanizing coating and 316L SS substrate have good adhesion due to the formation of the metallurgical bonding interfaces at different temperatures. This results from the interdiffusion of the alloying elements (e.g., Fe, Cr and Ni) in the substrate and the metallic element Ti in the powder mixture. The appearance of Al in the titanizing coating is caused by the tiny Al<sub>2</sub>O<sub>3</sub> particles embedded into the coating from the pack mixture [12, 13]. This demonstrates that the titanizing coating grows outwards, which is consistent with the growth model in the high-temperature low-activity process [14]. Therefore, the titanizing coating can be divided into an outer layer (OL) and an interdiffusion layer (IDL), as shown in Fig. 3(a-c). Fig. 3(a'-c') shows the detailed microstructure features of OL layers. It is seen that the outer layers consist of two sublayers with different thicknesses, i.e., thicker layer L1 and thinner outermost layer L2. In addition, many precipitates are dispersed in the OL layers. There are two phase regions with different contrast in the IDL layers.

**Table 2.** The EDS analysis results for the coating in Fig. 3(c and c') formed at 1100 °C (*at. %*)

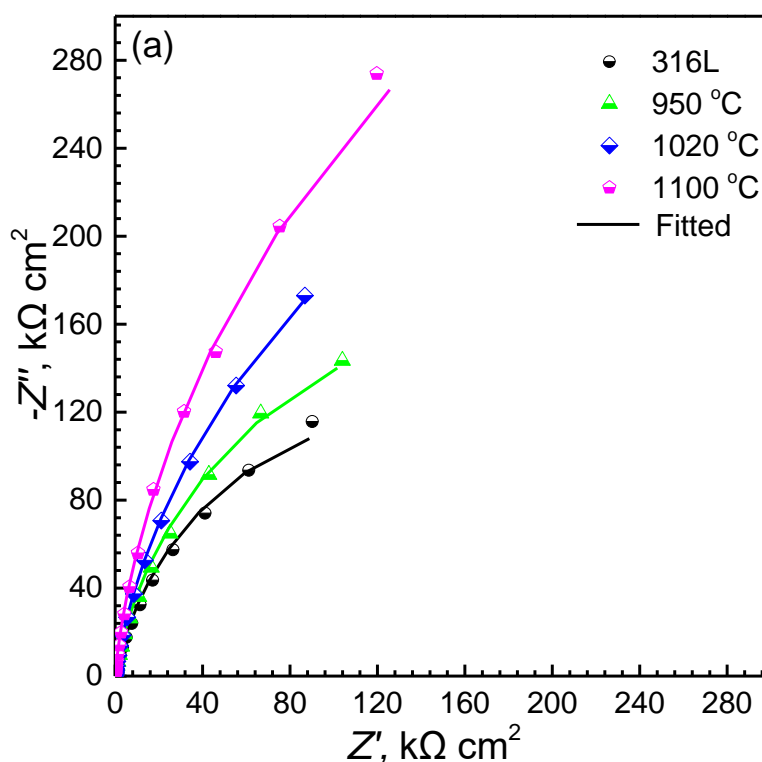
Layer	Location	Ti	Fe	Ni	Cr	Al	O	Si	Mo	Phase
L1	Point 1	44.1	5.9	2.9	0	17.9	29.2	0	0	Ti/NiTi <sub>2</sub>
	Point 2	37.8	15.3	8.1	0	13.4	25.4	0	0	
	Point 3	31.2	44.8	4.1	6.0	7.7	6.2	0	0	
L2	Point 4	36.3	21.9	9.4	2.4	11.2	18.8	0	0	NiTi
	Point 5	40.2	26.4	5.6	3.5	7.0	17.3	0	0	Precipitate
IDL	Point 6	10.6	59.7	5.6	19.2	0	0	1.9	3.1	Cr <sub>13</sub> Fe <sub>42</sub> Mo <sub>2</sub> Ti <sub>5</sub>
	Point 7	1.9	70.3	4.1	22.3	0	0	0.7	0.9	δ-Ferrite

As shown in Table 2, the Ti contents of both phases in the L2 layer are very high and decrease with the diffusion depth. Moreover, the Fe contents gradually increase as the coating grows. Based on the Walser-Bene rule, the first phase nucleated in metal-metal film reactions is directly close to the low-temperature eutectic point in the binary phase diagram [15]. Therefore, according to the Fe-Ti and Ni-Ti phase diagrams [16, 17] and the XRD and EDS results, it can be inferred that the L2 layer mainly consists of NiTi<sub>2</sub>/Ti, the brighter area is FeTi and the darker area is NiTi in the L1 layers. Additionally, the bright area is Cr<sub>13</sub>Fe<sub>42</sub>Mo<sub>2</sub>Ti<sub>5</sub> and the dark area is the δ-ferrite phase in the IDL layers. The uphill diffusion of Ni in Fig. 4 is caused by the formation of NiTi and NiTi<sub>2</sub> in the OL layers. Owing to the ability of Ti to deplete Ni (an austenite stabilizer), a localized austenite-to-ferrite phase transformation takes place at the advancing reaction front in the substrate [18]. The newly formed δ-ferrite phase then acts as a short-circuit path for the rapid diffusion of Ti atoms into the 316L SS substrate [18,19], resulting in the formation of a new phase Cr<sub>13</sub>Fe<sub>42</sub>Mo<sub>2</sub>Ti<sub>5</sub>. As the temperature increases from 950 to 1100 °C, the faster diffusion rate promotes the phase transformation process. As a result, the IDL and Cr<sub>13</sub>Fe<sub>42</sub>Mo<sub>2</sub>Ti<sub>5</sub> layers gradually become thicker with temperature. In addition, the precipitates in the OL layers mainly

consist of Ti and Fe. It is still unclear about their compound kinds, but the formation of precipitates is assumed to relieve supersaturation as the specimens are cooled from the processing temperature [19-21].

### 3.2 Electrochemical corrosion characteristics

Prior to the electrochemical experiments, the loose outermost layer was removed by slight polishing of each specimen surface. Fig. 5 presents the typical EIS diagrams for the titanizing coatings and 316L substrate at the corrosion potential in the 3.5% NaCl solution at 80 °C. The Nyquist curves show a similar feature for all the specimens with an incomplete capacitive semicircle (i.e., capacitive arc) within the whole frequency range. It is clear that the semicircle size for the titanizing coatings is much larger than that for 316L SS and increases as the temperature increases from 950 to 1100 °C. According to the Bode curves, the time constants from the charge transfer process at the low-frequency part and the passive film at the middle- and high-frequency parts overlap together as a horizontal platform with almost invariable phase angle  $\theta$  values in the range of 100 to 0.1 Hz. In more detail, the  $\theta$  values of the horizontal platform increase from approximately 80° to 85° with increasing temperature, which are higher than that of 316L SS (approximately 78°).



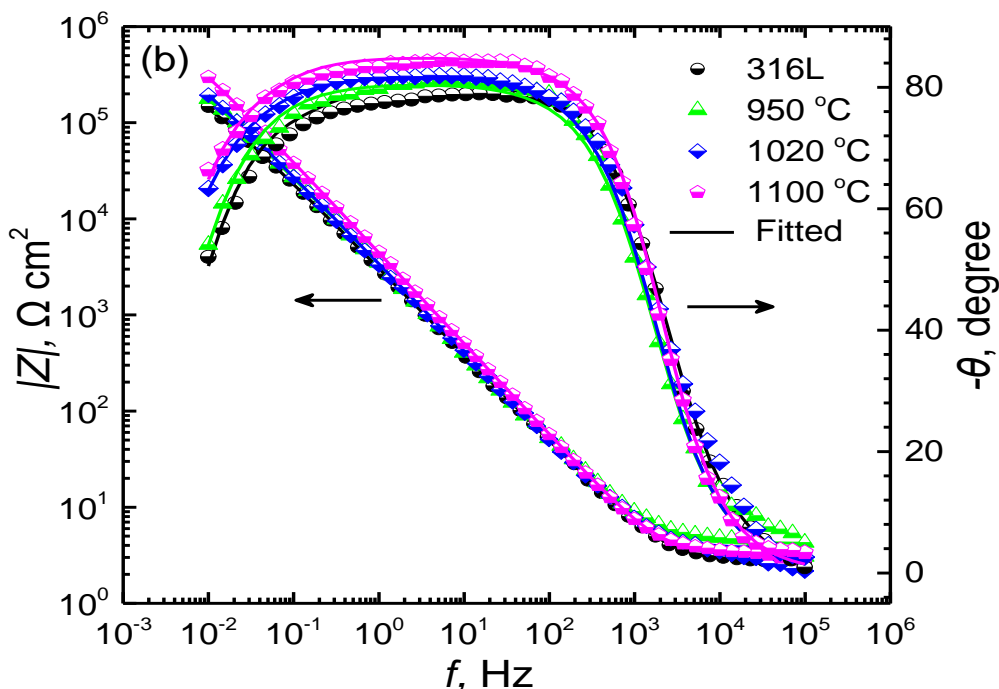


**Figure 5.** Typical EIS plots (a) Nyquist and (b) Bode for 316L SS and the titanizing coatings in 3.5% NaCl solution at 80 °C.

The equivalent circuit shown in Fig. 6 was used to fit the EIS spectra in Fig. 5, where  $R_s$  is the solution resistance,  $R_f$  and  $C_f$  represent the resistance and capacitance of the passive film, and  $R_t$  and  $C_{dl}$  represent the charge transfer resistance and double layer capacitance, respectively. The constant phase element (CPE) was adopted to substitute all the capacitance elements in the fitting procedure because of the nonideal capacitive response of the SS/solution interface [22]. The impedance of CPE is expressed as

$$Z_{CPE} = \frac{1}{Y_0(j\omega)^\alpha} \quad (1)$$

where  $Y_0$  is the admittance magnitude of CPE, and  $\alpha$  is the exponential term [22, 23].

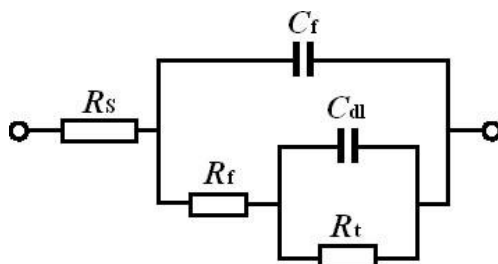


**Figure 6.** Equivalent circuit for the electrode system 316L SS/NaCl solution

The fitted values from the EIS spectra are listed in Table 3. The polarization resistance  $R_p$  (i.e., corrosion resistance) theoretically equals the sum of  $R_t$  and  $R_f$  [23, 24].  $R_s$  remains almost constant with

a value of approximately 3 to 4  $\Omega \text{ cm}^2$  because of the strong conductivity of the test solution. All specimens exhibit good corrosion resistance with very large  $R_p$  values on the order of  $10^5$  to  $10^6 \Omega \text{ cm}^2$ . This indicates that protective passive films formed on the specimen surfaces. It is clear that the  $R_p$  values of the titanizing coatings are higher than that of the 316L SS substrate. This can be primarily attributed to the formation of the  $\text{TiO}_2$  film in the test solution and significantly increases the corrosion resistance [25], revealing the excellent protectiveness of the titanizing coatings. Moreover, as the titanizing temperature increases from 950 to 1100  $^\circ\text{C}$ , the  $R_p$  value gradually increases, but the  $Y_{0-f}$  and  $Y_{0-dl}$  values continuously decrease. These results clearly indicate that the titanizing coatings have much higher corrosion resistance than the uncoated 316L SS, and the higher the titanizing temperature is, the higher the corrosion resistance in the test solution.

**Table 3.** Fitting results of electrochemical impedance spectroscopy

Specimen	$R_s$ ( $\Omega \text{ cm}^2$ )	$Y_{0-f}$ ( $10^{-5} \text{S}^\alpha \Omega \text{ cm}^{-2}$ )	$\alpha_f$	$Y_{0-dl}$ ( $10^{-5} \text{S}^\alpha \Omega \text{ cm}^{-2}$ )	$\alpha_{dl}$	$R_p$ ( $10^5 \Omega \text{ cm}^2$ )
316LSS	2.75	6.27	0.90	9.00	0.90	2.74
950 $^\circ\text{C}$	4.21	5.67	0.90	4.92	0.91	3.80
1020 $^\circ\text{C}$	3.78	5.53	0.91	2.27	0.88	6.35
1100 $^\circ\text{C}$	3.30	3.97	0.90	2.16	0.99	9.03

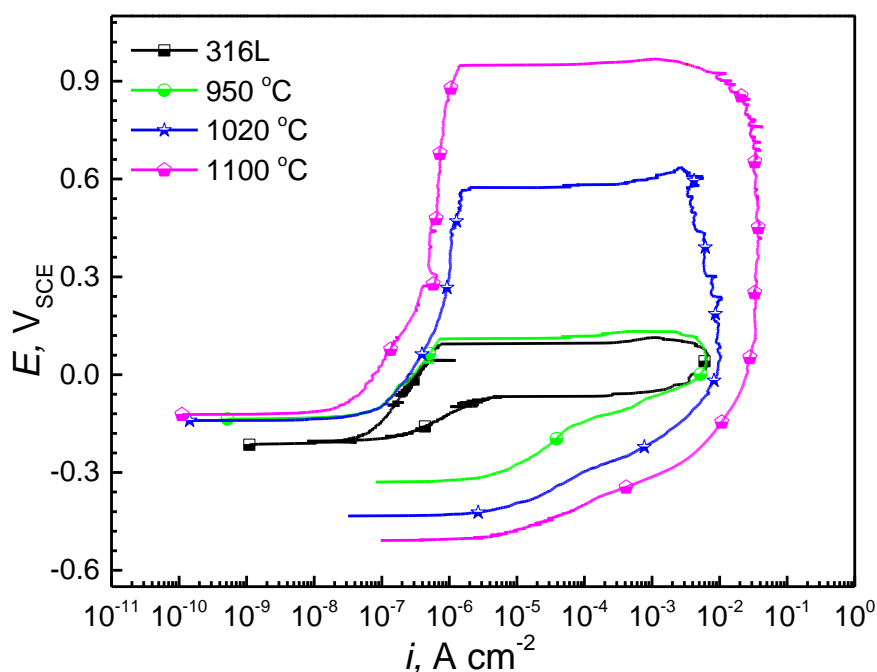


**Figure 7.** Cyclic anodic polarization curves of specimens in 3.5% NaCl solution at 80  $^\circ\text{C}$

Fig. 7 shows the cyclic anodic polarization curves of the 316L SS substrate and titanizing coating in a 3.5% NaCl solution at 80  $^\circ\text{C}$ . Both the coated and uncoated 316L SS specimens can passivate spontaneously, and the passive current decreases gradually with increasing titanization temperature. The

current density will increase suddenly when the electrode potential rises to a limit value, revealing the breakdown of the passive film and the subsequent occurrence of stable pitting corrosion. Obviously, the pitting potential ( $E_p$ ) of the coated specimens is always higher than that of the 316L SS substrate, and the  $E_p$  value shifts positively from  $113\pm 14$  to  $950\pm 42$  mV<sub>SCE</sub> with increasing titanization temperature from 950 to 1100 °C. These results are in good agreement with the EIS results.

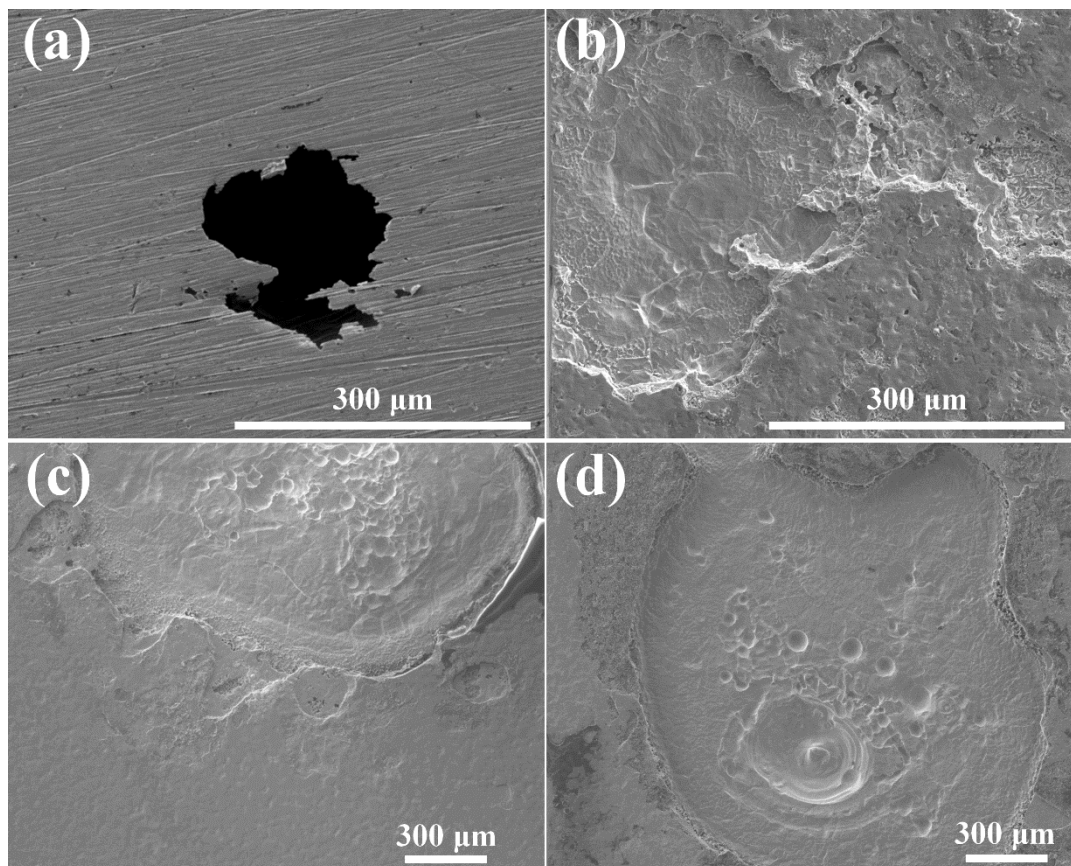


**Figure 8.** SEM morphologies of the pits on different samples after the cyclic anodic polarization test: (a) 316L SS and titanized 316L at (b) 950 °C, (c) 1020 °C, (d) 1100 °C

Figs. 8 and 9 give the surface and cross-sectional images of the pits on different specimens after the cyclic anodic polarization test, respectively. It is apparent that the stable pits on the coated and uncoated specimens present different features. For the 316L SS substrate, the stable pits show small widths but large depths with some undermined metallic covers over the pit mouths. However, the pits formed on titanizing specimen surfaces are much larger with a maximum width of approximately several millimeters and display a typical shallow dish shape with a small depth/radius ratio [26]. It has been reported that NiTi<sub>2</sub> and metallic Ti exhibit excellent corrosion resistance in 3.5% NaCl solution while NiTi and ferrite exhibit the opposite [27-29]. It can be inferred that the presence of Ti and NiTi<sub>2</sub> in the outermost layer is the main reason for the high corrosion resistance of the titanizing specimens. In addition, the increase in titanizing temperature results in a thicker Ti/NiTi<sub>2</sub> layer, so the coatings exhibit better protectiveness with higher  $E_p$  and  $R_p$  values. Furthermore, it can be seen from Fig. 9(d) that NiTi will dissolve preferentially when the Ti/NiTi<sub>2</sub> layer is destroyed. However, the higher Mo and Ti contents

must result in higher corrosion resistance for the  $\text{Cr}_{13}\text{Fe}_{42}\text{Mo}_2\text{Ti}_5$  phase in comparison with the ferritic phase. As a result, selective dissolution of the ferritic phase took place when pitting corrosion propagated into the IDL. The corrosion resistance difference between the phases is mainly responsible for the faster growth of pits in the horizontal direction and the formation of a shallow dish shape. Therefore, it is necessary to further optimize the titanizing process and control the phase composition of the titanizing coatings to reduce the influence of weaker phases on the corrosion resistance. In addition, the stable pits on the titanizing specimens at 1020 and 1100 °C will grow into very large sizes and even propagate into the matrix. This can be attributed to the higher  $E_p$  values. Active dissolution always occurs in the stable pits before repassivation, and the higher the polarization potential is, the more intense the active dissolution. Therefore, if the stable pit was polarized from a higher initial potential (i.e.,  $E_p$ ), a larger current density may be generated for pit propagation during the reverse scan and impede the repassivation process, as shown in Fig. 7. This is similar to the result for 2205 duplex stainless steel in hot concentrated seawater [22].

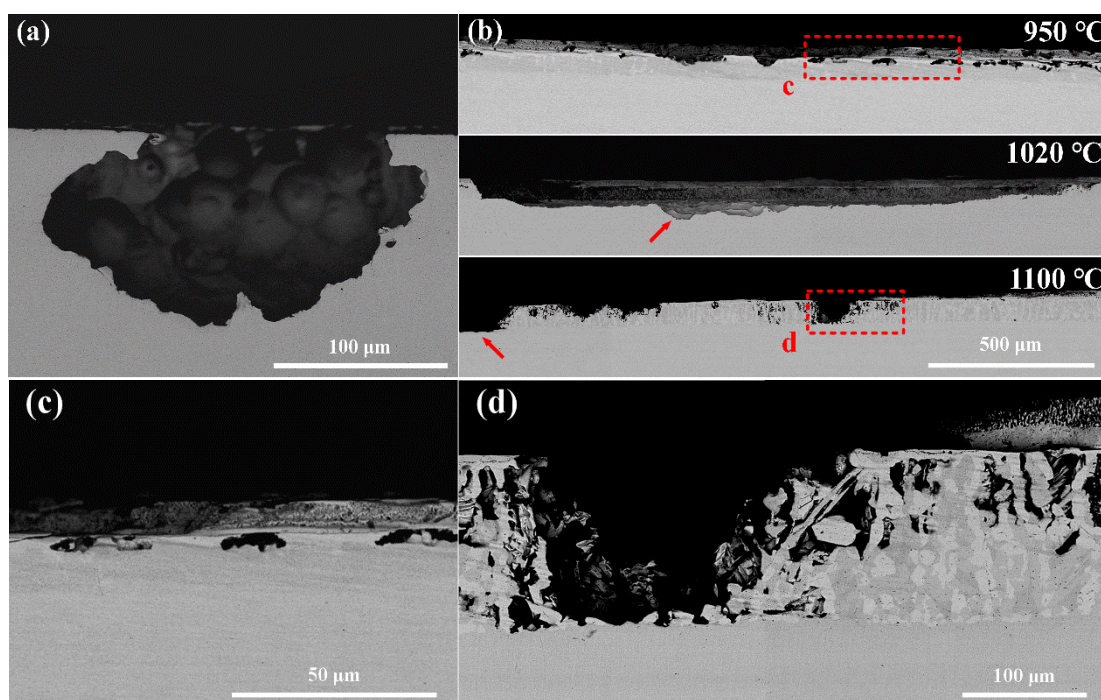


**Figure 9.** Cross-sectional images of the stable pits for (a) 316L SS, (b) the titanizing coatings and the enlarged positions marked on the coatings at (c) 950 °C and (d) 1100 °C.

#### 4. CONCLUSIONS

Dense titanizing coatings were prepared on 316L SS via pack cementation at 950 to 1100 °C for 3 h. The coatings consisted of two layers. The outer layer comprises Ti and intermetallic compound phases such as  $\text{NiTi}_2$ ,  $\text{FeTi}$  and  $\text{NiTi}$ , while the inner layer is an interdiffusion layer of  $\delta$ -ferrite and  $\text{Cr}_{13}\text{Fe}_{42}\text{Mo}_2\text{Ti}_5$ . Additionally, the titanizing coatings are tightly adhered to the 316L SS substrate.

The titanizing coatings exhibit excellent spontaneous passivation performance in 3.5% NaCl solution at 80 °C. By changing the packing temperature from 950 to 1100 °C, both the polarization resistance and pitting potential become significantly higher. Obviously, the titanizing coatings can provide good protection for 316L SS in aggressive brine environments. The constituent phases of titanizing coatings display different corrosion resistances and the high corrosion properties primarily result from the Ti/NiTi<sub>2</sub> phases in the outer layer.

## References

1. Y. Shang, Y. Yuan, D. Li, Y. Li, J. Chen, *Int. J. Adv. Manuf. Tech.*, 92 (2017) 4379.
2. G.T. Gray, V. Livescu, P.A. Rigg, C.P. Trujillo, C.M. Cady, S.R. Chen, J.S. Carpenter, T.J. Lienert and S.J. Fensin, *Acta Mater.*, 138 (2017) 140.
3. W. Tian, N. Du, S. Li, S. Chen and Q. Wu, *Corros. Sci.*, 85 (2014) 372.
4. D. Starosvetsky, I. Gotman, *Surf. Coat. Tech.*, 148 (2001) 268-276.
5. R. Mevrel, C. Duret and R. Pichoir, *Mater. Sci. Tech-Lond.*, 2 (1986) 201.
6. R. Bianco, R.A. Rapp, Pack cementation diffusion coatings. In: Stern K.H. (eds) *Metallurgical and Ceramic Protective Coatings*, Springer, (1996) Dordrecht, Netherlands.
7. J.C. Liu, G. Zhang, J.S. Ma and K. Suganuma, *J. Alloy. Compd.*, 644 (2015) 113.
8. N.M. Lin, L. Zhao, Q. Liu, J. Zou, R. Xie, S. Yuan, D. Li, L. Zhang, Z. Wang and B. Tang, *J. Phys. Chem. Solids.*, 129 (2019) 387.
9. X.G. Xing, H. Wang, P. Lu and Z. Han, *Surf. Coat. Tech.*, 291 (2016) 151.
10. S.S. Xin, M.C. Li, *Corros. Sci.*, 81 (2014) 96.
11. N.M. Lin, F. Xie, H. Yang, W. Tian, H. Wang and B. Tang, *Appl. Surf. Sci.*, 258 (2012) 4960.
12. X.M. Peng, C.Q. Xia, Y.Y. Liu and J.H. Wang, *Surf. Coat. Tech.*, 203 (2009) 3306.
13. G. Hu, Z. Xu, J. Liu and Y. Li, *Surf. Coat. Tech.*, 203 (2009) 3392.
14. J. R. Nicholls, K. A. Long and N. J. Simms, *Anti-Corros. Method. M.*, 13 (1966) 21
15. R.W. Bené, *Appl. Phys. Lett.*, 41 (1982) 529.
16. O. Kubaschewski, *IRON-Binary Phase Diagrams*, Springer, (1982) Berlin, Germany.
17. J. L. Murray. *ASM. Internationl, Materials Park, Ohio.* (1991)
18. N. Bangaru, R. Krutenat, *Surf. Eng.*, 85 (1984) 427.
19. S.C.K. D. M. Miller, S. D. Scarberry and R. A. Rapp, *Oxid. Met.*, 29 (1988) 239.
20. N. Bangaru, R. Krutenat, *J. Vac. Sci. Technol. B.*, 2 (1984) 806.
21. A.E.P.y. Puentea, D.C. Dunandb, *Intermetallics*, 92 (2018) 42.
22. Y. Yang, H.T. Zeng, S.S. Xin, X.L. Hou and M.C. Li, *Corros. Sci.*, 165 (2020) 108383.
23. H.T. Zeng, Y. Yang, M.H. Zeng and M.C. Li, *J. Mater. Sci. Technol.*, 66 (2021) 177.
24. M.C. Li, S.Z. Luo, P.F. Wu and J.N. Shen, *Electrochim. Acta*, 50 (2005) 3401.
25. J. Guo, Y. Yang, Q. Zhu, C. Fan, P. Lv and M. Xiang, *Surf. Coat. Tech.*, 353 (2018) 18.
26. C. Pan, L. Liu, Y. Li and F. Wang, *Corros. Sci.*, 73 (2013) 32.
27. A. Sedriks, J. Green and D.J.C. Novak, *Corrosion*, 28 (1972) 137.
28. J.J. Marattukalam, V.K. Balla, M. Das and S. Bontha, *J. Alloy. Compd.*, 744 (2018) 337.
29. D. Wever, A. Veldhuizen, J. De Vries, H. Busscher, D. Uges and J.J.B. Van Horn, *Biomaterials*, 19 (1998) 761.